

Data-Enhanced Variational Monte Carlo Simulations for Rydberg Atom Arrays

Stefanie Czischek,^{1,*} M. Schuyler Moss,¹ Matthew Radzihovsky,^{2,†} Ejaaz Merali,^{1,3} and Roger G. Melko^{1,3}

¹*Department of Physics and Astronomy, University of Waterloo, Ontario, N2L 3G1, Canada*

²*Department of Physics, Stanford University, Stanford, CA 93405, USA*

³*Perimeter Institute for Theoretical Physics, Waterloo, Ontario, N2L 2Y5, Canada*

(Dated: May 11, 2022)

Rydberg atom arrays are programmable quantum simulators capable of preparing interacting qubit systems in a variety of quantum states. Due to long experimental preparation times, obtaining projective measurement data can be relatively slow for large arrays, which poses a challenge for state reconstruction methods such as tomography. Today, novel groundstate wavefunction ansätze like recurrent neural networks (RNNs) can be efficiently trained not only from projective measurement data, but also through Hamiltonian-guided variational Monte Carlo (VMC). In this paper, we demonstrate how pretraining modern RNNs on even small amounts of data significantly reduces the convergence time for a subsequent variational optimization of the wavefunction. This suggests that essentially any amount of measurements obtained from a state prepared in an experimental quantum simulator could provide significant value for neural-network-based VMC strategies.

I. INTRODUCTION

Rydberg atom arrays are powerful candidates for high-quality quantum simulation and computing platforms [1–3]. State-of-the-art experiments use optical tweezers to arrange and individually address atoms on arbitrary lattices [4–6], allowing them to strongly interact with a many-body Hamiltonian [7]. The combination of complex lattice structures together with the precise tuning of inter-atomic interactions has enabled the preparation of various novel phases and phase transitions [6, 8, 9], whose continuing experimental exploration is supported by a suite of rapidly advancing numerical simulation technologies [10–14].

The quantum state of an array is probed with fluorescent imaging techniques, which provide projective measurements in the Rydberg occupation basis [4, 6, 15]. Since each measurement is destructive, the repetition rate at which they can be performed is limited by a number of factors, in particular the preparation time of the target quantum state. The probabilistic loading of the array requires a non-trivial rearrangement of atoms, resulting in repetition rates on the order of a few measurements per second [4, 6], with exact time scales depending on the specific experimental setup. Thus, data acquisition is limited, especially when compared to competing quantum simulation platforms, such as ion traps which allow for hundreds of measurements per second [16], or superconducting circuits where orders of magnitude more measurements per second can be achieved [17].

Data acquisition rates have obvious consequences for state reconstruction and characterization, as well as the direct estimation of operator expectation values, which suffer variances that scale inversely proportional to the

number of independent measurements. Recently, neural network wavefunctions have been explored as tools for leveraging limited measurement data, as they provide a powerful ansatz for representing quantum states with systematically tunable expressivity [18–24]. For example, standard generative models adopted from the field of machine learning have been used to tomographically reconstruct quantum states [25–31] and have demonstrated the ability to significantly reduce the amount of measurements required for the accurate reconstruction of operator expectation values [25]. In addition to their designed ability for *data-driven* learning, these ansätze have the ability to find ground state wavefunctions of a given Hamiltonian by variational energy minimization, via the same *Hamiltonian-driven* training methods common in variational Monte Carlo (VMC) [32–34]. Modern neural network strategies provide VMC ansätze that can systematically be made powerful enough that their expressiveness is no longer the limiting bottleneck. Instead, the optimization process often requires long convergence times [35–39] and physics-inspired modifications of the network structure are sometimes needed to reach accuracies comparable to traditional VMC approaches [40, 41]. In addition, the power of wisely chosen initializations to improve convergence has already been demonstrated in traditional VMC methods [42, 43].

In this work, we leverage these unique features of neural network wavefunctions to explore the effect of combined data- and Hamiltonian-driven learning [44]. Beginning with a randomly initialized recurrent neural network (RNN) [23], we first optimize network parameters using a limited amount of simulated [12, 14, 45] Rydberg occupation data drawn from a two-dimensional array in the vicinity of a quantum phase transition. Then, we continue optimizing the network variationally, in the spirit of the recent work by Carrasquilla and Torlai [33]. We find a significant enhancement in variationally obtaining the ground state wavefunction by pretraining the RNN on a limited amount of quantum data.

* sczischek@uwaterloo.ca

† Currently at Apple Inc. One Apple Park Way, Cupertino, CA 95014, USA

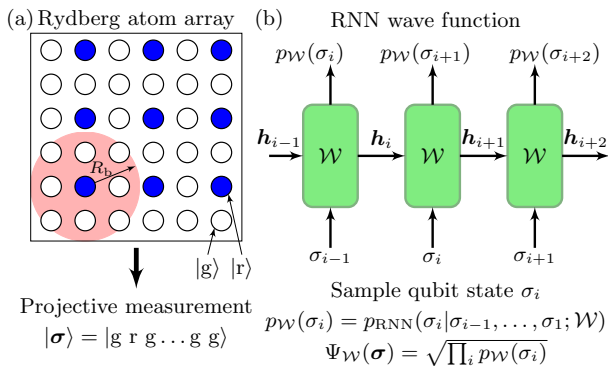


FIG. 1. (a) Square lattice of 6×6 atoms in the *striated* phase, where atoms in the Rydberg state (blue) are separated by stripes of atoms in the ground state (white) due to the Rydberg blockade radius R_b . Projective measurements of individual atoms in the occupation number basis provide information about the quantum state. (b) A recurrent neural network (RNN), with green boxes representing a cell with N_h hidden units and tunable parameters \mathcal{W} . An input sequence σ is iteratively provided to the network, generating an output depending on the current input σ_i and the hidden unit state h_i . A single qubit state is used as input at iteration i and the network output is the probability distribution underlying the state of qubit $i+1$, from which the input σ_{i+1} is sampled [23].

II. BACKGROUND

We consider a system of $N = L \times L$ atoms arranged on a square lattice with spacing $a = 1$ and open boundary conditions [Fig. 1(a)]. Each atom can be found in a ground state $|g\rangle$ or in an excited (Rydberg) state $|r\rangle$. The system is driven by the many-body Hamiltonian,

$$\hat{H} = -\frac{\Omega}{2} \sum_{i=1}^N \hat{\sigma}_i^x - \delta \sum_{i=1}^N \hat{n}_i + \sum_{i,j} V_{ij} \hat{n}_i \hat{n}_j, \quad (1)$$

with off-diagonal operator $\hat{\sigma}_i^x = |g\rangle_i \langle r|_i$, and occupation operator $\hat{n}_i = |r\rangle_i \langle r|_i$ acting on atom i . Atoms at positions \mathbf{r}_i and \mathbf{r}_j interact via the van der Waals potential $V_{ij} = \Omega R_b^6 / |\mathbf{r}_i - \mathbf{r}_j|^6$, where the Rydberg blockade radius R_b defines a region within which simultaneous excitations are penalized [46, 47]. Individual atoms are driven by a coherent laser with detuning δ and Rabi frequency Ω . We fix $\delta = \Omega = 1$ and $R_b = 7^{1/6}$, so that $V_{ij} = 7/|\mathbf{r}_i - \mathbf{r}_j|^6$, in the following. This brings the system in the vicinity of the transition between the disordered and the striated phase [6].

Information about the quantum state of a Rydberg array can be obtained from projective measurements in the occupation basis, which gives full information about the positive real-valued ground state wavefunction of Eq. (1) [4, 6, 15]. Each measurement forces a wavefunction collapse and the target state needs to be re-prepared before the next measurement can be performed.

Given sufficient projective measurements, a quantum state can be tomographically reconstructed, e.g. via a

neural network wavefunction ansatz [20–22, 25–28, 33, 48, 49]. Here, we focus on RNNs to represent quantum states, as illustrated in Fig. 1(b), and choose the gated recurrent unit (GRU) [50] as network cell, inspired by Refs. [23, 33]. The RNN generates an output based on a sequence of inputs σ and the state of N_h hidden neurons per network cell. During the training process, the network parameters \mathcal{W} are tuned to generate a target output. The amount of tunable parameters is defined by N_h , which can be increased to improve the network expressivity. More details on RNNs are given in [23, 33, 50].

RNNs are naturally designed to encode probability distributions [23]. The network output at iteration i can be interpreted as the conditional probability distribution $p_{\text{RNN}}(\sigma_i | \sigma_{i-1}, \dots, \sigma_1; \mathcal{W})$, providing the joint distribution $p_{\text{RNN}}(\sigma; \mathcal{W}) = \prod_i p_{\text{RNN}}(\sigma_i | \sigma_{i-1}, \dots, \sigma_1; \mathcal{W})$. To represent a wavefunction, single qubit states are chosen as network input, which is iterated over the entire qubit system. The RNN is then trained to encode the probability distribution underlying projective measurements in the computational basis. In the case of positive real-valued wavefunctions, such as the ground state of Eq. (1), the RNN represents the full quantum state $\Psi_{\mathcal{W}}(\sigma) = \langle \sigma | \Psi \rangle = \sqrt{p_{\text{RNN}}(\sigma; \mathcal{W})}$. Further modifications can be used to reconstruct arbitrary complex wavefunctions or density matrices [23, 33].

Finally, samples from the generative step of the RNN-encoded distribution emulate projective measurement outcomes. The quantum state of the full system can be sampled by iteratively drawing single qubit states. We use these samples to evaluate the energy expectation value $H_{\text{RNN}} = \langle \Psi_{\mathcal{W}} | \hat{H} | \Psi_{\mathcal{W}} \rangle$ via,

$$H_{\text{RNN}} = \sum_{\{\sigma\}} |\Psi_{\mathcal{W}}(\sigma)|^2 H_{\text{loc}}(\sigma) \approx \frac{1}{N_s} \sum_{\sigma \sim p_{\text{RNN}}(\sigma; \mathcal{W})} H_{\text{loc}}(\sigma), \quad (2)$$

where we introduce the local energy,

$$H_{\text{loc}}(\sigma) = \frac{\langle \sigma | \hat{H} | \Psi_{\mathcal{W}} \rangle}{\langle \sigma | \Psi_{\mathcal{W}} \rangle}, \quad (3)$$

which is calculated and averaged over N_s samples σ drawn from $p_{\text{RNN}}(\sigma; \mathcal{W})$ and can efficiently be evaluated for local non-diagonal operators [19, 20, 23, 32, 33].

III. RNN TRAINING PROCEDURES

We first explore the reconstruction of the ground state of a Rydberg atom array based on a projective measurement data set \mathcal{D} . In this data-driven setting, we optimize an RNN to approximate the probability distribution $p_{\text{RNN}}(\sigma) \approx p_{\mathcal{D}}(\sigma)$ underlying the data points $\sigma \in \mathcal{D}$. We use the Kullback-Leibler divergence to define the loss

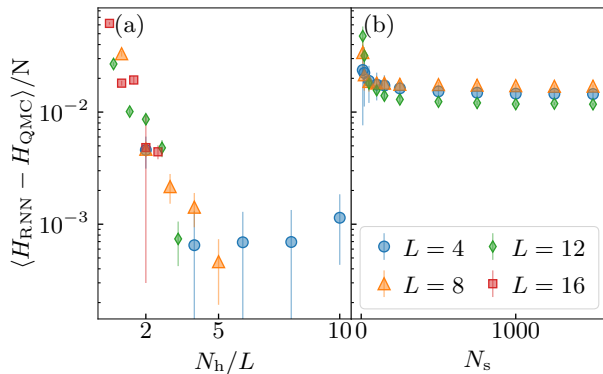


FIG. 2. (a) Energy density difference of data-driven trained RNN states for different system sizes $N = L \times L$ as a function of the number of hidden neurons N_h per network cell. Results are averaged over iterations 1350 to 1400 (950 to 1000 for $N = 16 \times 16$) and error bars denote standard deviations. The RNN is trained on 10^5 data points with learning rate $\eta = 10^{-4}$. (b) Energy density difference of an RNN trained with the Hamiltonian-driven procedure using $\eta = 10^{-3}$. Results are plotted versus the number of RNN samples N_s for different system sizes, with $N_h = 2L$. Data is averaged over iterations 950 to 10,000 with standard deviations as error bars. The QMC energy densities are $L = 4$: $H_{\text{QMC}}/16 = -0.4534(1)$, $L = 8$: $H_{\text{QMC}}/64 = -0.4052(2)$, $L = 12$: $H_{\text{QMC}}/144 = -0.3885(2)$, $L = 16$: $H_{\text{QMC}}/256 = -0.3805(2)$.

function,

$$\mathcal{L}_{\text{DKL}}(\mathcal{W}) = \sum_{\{\sigma\}} p_{\mathcal{D}}(\sigma) \log \frac{p_{\mathcal{D}}(\sigma)}{p_{\text{RNN}}(\sigma; \mathcal{W})} \quad (4)$$

$$\approx -S_{\mathcal{D}} - \frac{1}{|\mathcal{D}|} \sum_{\sigma \in \mathcal{D}} \log p_{\text{RNN}}(\sigma; \mathcal{W}). \quad (5)$$

In the last line we approximate $p_{\mathcal{D}}$ with the sum over the data in \mathcal{D} and introduce the entropy $S_{\mathcal{D}} = -\sum_{\{\sigma\}} p_{\mathcal{D}}(\sigma) \log p_{\mathcal{D}}(\sigma)$. We use the Adam optimizer [51] to train a Glorot uniform initialized [52] RNN by determining parameters \mathcal{W} that minimize the loss function.

In order to produce a dataset \mathcal{D} , we use the quantum Monte Carlo (QMC) algorithm introduced in [14], which is able to accurately emulate projective measurements of Rydberg atoms in the ground state of the Hamiltonian in Eq. (1). We consider systems with up to $N = 16 \times 16$ atoms, relevant for state-of-the-art experimental realizations [6], for which an unbiased estimate of the energy H_{QMC} is easily obtained. We generate $|\mathcal{D}| = 10^5$ QMC samples for all considered system sizes, which gives estimates of the ground state energy density H_{QMC}/N with errors on the order of $\sim 10^{-4}$ (caption of Fig. 2).

We implement our RNN based on the code provided in [33, 53] and choose similar network hyperparameters, fixing the learning rate to $\eta = 0.001$ unless otherwise stated. We first analyze the expressivity of the RNN in the data-driven approach to training. In Fig. 2(a) we

train the network on the entire set of $|\mathcal{D}| = 10^5$ QMC data points for different system sizes of $N = L \times L$ atoms and plot the energy density difference $\langle H_{\text{RNN}} - H_{\text{QMC}} \rangle / N$ as a function of the number of hidden neurons N_h per network cell. The energy density differences are averaged over optimization iterations 1350 to 1400, where the training is approximately converged. Each iteration corresponds to one training epoch where the full input dataset is given to the RNN in batches of 100 randomly chosen samples and the network parameters are updated. The energy expectation value H_{RNN} is calculated on 1000 samples drawn from $p_{\text{RNN}}(\sigma; \mathcal{W})$. For $N = 16 \times 16$ we average the energy densities over iterations 950 to 1000 due to long computational runtimes, leading to larger variances as convergence is not yet reached. For all system sizes the energy density error shows a clear decreasing trend with increasing N_h , which corresponds to higher network expressivity. We find that the observed differences reach values below 10^{-2} for $N_h/L \geq 2$ in all cases. While higher reconstruction accuracies can be reached, increasing N_h comes at the price of higher computational costs. We thus focus on $N_h = 2L$ as a practical compromise in the following.

Next, we train the RNN to represent the ground state of the same $N = L \times L$ system using the Hamiltonian-driven approach. In this procedure, the RNN parameters are optimized such that the energy expectation value H_{RNN} is minimized, corresponding to VMC. With this motivation we define the loss function,

$$\mathcal{L}_H(\mathcal{W}) = \frac{1}{N_s} \sum_{\sigma \sim p_{\text{RNN}}(\sigma; \mathcal{W})} H_{\text{loc}}(\sigma), \quad (6)$$

and use again the Adam optimizer [51] to find optimal network parameters \mathcal{W} . Here we evaluate the local energy, Eq. (3), on N_s samples drawn from $p_{\text{RNN}}(\sigma; \mathcal{W})$.

In Fig. 2(b) we consider the energy density difference as a function of N_s for different system sizes. The largest system size, $N = 16 \times 16$, is not shown due to exceeding computational runtimes. We choose $N_h = 2L$ and average the measured energy densities over optimization iterations 9500 to 10,000. The measured differences decrease with increasing N_s , before they saturate at $\sim 10^{-2}$ for $N_s \geq 500$. In accordance with [33] we thus fix $N_s = 1000$ in the following. All system sizes show larger energy density differences than in Fig. 2(a). This demonstrates the limitation of the Hamiltonian-driven training procedure even after a large number of iterations, which require prohibitively long computation times. This large amount of required optimization steps is commonly caused by local optima in the parameter landscape and has led to various model-inspired modifications of VMC [35, 37–39, 42, 43]. Below, we show that variational optimization can incur significant performance improvements without system-specific modifications, by finding suitable initializations resulting from data-driven pretraining.

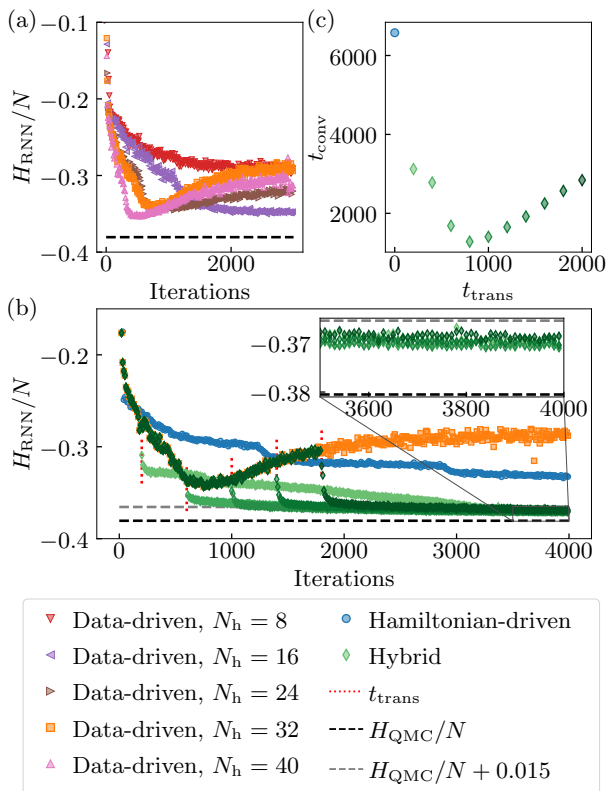


FIG. 3. Quantum state reconstruction of an $N = 16 \times 16$ atom array. (a) Energy density H_{RNN}/N as a function of optimization iterations using the data-driven training on 1000 data points. Different shapes and colors show different N_h compared to the target energy density H_{QMC}/N . (b) Energy density evolution during data-driven, Hamiltonian-driven, and hybrid training with different t_{trans} (darker green shows larger t_{trans}) and $N_h = 32$. Inset emphasizes the convergence to the target solution after ≥ 3500 iterations within a margin of 0.015 for all $t_{\text{trans}} > 0$. (c) Convergence time t_{conv} (see main text for definition) as a function of transition point t_{trans} in the hybrid training of an RNN with $N_h = 32$.

IV. DATA-ENHANCED VMC

In the above, we have shown that RNN wavefunctions can be made sufficiently expressive to represent the ground state of large Rydberg arrays, however naive variational optimization of the neural network parameters does not lead to accurate energies in a reasonable amount of simulation time. Further, due to the long state-preparation times in modern Rydberg experiments [4, 6], it is reasonable to hypothesize that accurate data-driven reconstruction will be challenging on large arrays due to limited data. To test this, we generate a randomly chosen subset of \mathcal{D} containing 1000 projective Rydberg occupation measurements, representing a typical amount of experimental data. In Fig. 3(a) we show the energy density expectation value when training networks with different numbers of hidden neurons N_h on the Rydberg

ground state of $N = 16 \times 16$ atoms. Instead of converging towards the estimated value, the energies for $N_h \geq 24$ reach a minimum at ~ 700 iterations. This phenomenon is easily recognized as overfitting.

Clearly, such limited datasets are insufficient for accurate state reconstruction. However, we now demonstrate the ability of small datasets to enhance the performance of VMC in a *hybrid* training procedure, defined with a simple change of loss function. Namely, we begin training the RNN with the data-driven loss function Eq. (5), before switching to Hamiltonian-driven training via Eq. (6) after t_{trans} iterations. Fig. 3(b) illustrates the effectiveness of this simple hybrid procedure. The green diamonds show the evolution of the energy using 1000 data points in data-driven training, before switching to Hamiltonian-driven training after t_{trans} iterations. As a comparison, we also plot purely Hamiltonian-driven training results (i.e. $t_{\text{trans}} = 0$). We explore a number of different choices of t_{trans} , which show significantly better convergence than the pure Hamiltonian-driven variational method out to 4000 optimization steps. All hybrid-trained simulations reach similar energy densities at $\gtrsim 3500$ iterations, which approximate the estimated value within a margin of 0.015 (see Fig. 3(b) inset).

In order to quantify the performance improvement of our algorithm, we define a convergence time t_{conv} as the iteration after which the energy density difference reaches $(H_{\text{RNN}} - H_{\text{QMC}})/N \leq 0.015$ for the first time. Results are illustrated in Fig. 3(c), where for better accuracy we consider the running average over 50 iterations, $\frac{1}{50} \sum_{i=-24}^{25} H_{\text{RNN}}(t+i)$, with t denoting the iterations. The convergence time is significantly reduced for all $t_{\text{trans}} > 0$, while Hamiltonian-driven training converges after $t_{\text{conv}} \sim 6600$ iterations. The shortest convergence time for our hybrid algorithm is observed for $t_{\text{trans}} = 800$, which is around the minimum of the data-driven training curve. Numerical studies on smaller system sizes have shown similar improvements in the hybrid training approach. While overfitting in the data-driven training starts at different points for different system sizes and amounts of hidden neurons, Fig. 3(c) proposes that t_{trans} does not need to be optimized to ensure convergence within reasonable computational runtimes.

V. CONCLUSIONS

In this paper, we have explored the use of recurrent neural networks (RNNs) for studying ground state wavefunctions of interacting Rydberg atom arrays of sizes currently accessible to experiments. We consider RNNs both trained from projective measurement data that could be produced by a typical experiment, as well as trained variationally with knowledge of the target Hamiltonian. In the latter, we show that naive variational training of RNNs becomes challenging for arrays approaching current experimental sizes. However, we find that RNNs which undergo a preliminary training phase driven by

a small amount of measurement data converge to accurate ground state energies with significantly less optimization steps than RNNs optimized without access to data. This result indicates the value of projective measurement data, obtained from Rydberg arrays and other quantum simulators, as a mechanism to significantly improve the convergence times of variational Monte Carlo simulations. This strategy should be immediately accessible to RNNs and other neural network wavefunction ansätze, which are amenable to both data-driven and Hamiltonian-driven training.

Our work also clearly indicates that the current generation of Rydberg atom arrays can produce data of high value to physicists, even at measurement rates which may be too low to be informationally complete for a full tomographic reconstruction of the quantum state. This strategy can be combined with the recent observation that Hamiltonian-driven optimization can also be used to mitigate errors in noisy experiments [44]. This suggests that the current generation of quantum hardware is on the cusp of bringing transformative improvement to the understanding of challenging quantum many-body

systems, by providing data to enhance variational simulation strategies for any state that can be prepared by an experimental quantum simulator.

ACKNOWLEDGEMENTS

We thank J. Carrasquilla, E. Inack, I. De Vlucht, M. P. A. Fisher, D. Sels, R. Luo, and Y. H. Teoh for critically important discussions. Simulations were made possible by the facilities of the Shared Hierarchical Academic Research Computing Network (SHARCNET) and Compute Canada. This work was supported by NSERC, the Canada Research Chair program, the New frontiers in Research Fund, and the Perimeter Institute for Theoretical Physics. Research at Perimeter Institute is supported in part by the Government of Canada through the Department of Innovation, Science and Economic Development Canada and by the Province of Ontario through the Ministry of Economic Development, Job Creation and Trade.

-
- [1] P. Scholl, M. Schuler, H. Williams, A. Eberharter, D. Barredo, K.-N. Schymik, V. Lienhard, L.-P. Henry, T. Lang, T. Lahaye, A. Läuchli, and A. Browaeys, Quantum simulation of 2D antiferromagnets with hundreds of rydberg atoms, *Nature* **595**, 233 (2021).
- [2] I. Cong, S.-T. Wang, H. Levine, A. Keesling, and M. D. Lukin, Hardware-efficient, fault-tolerant quantum computation with rydberg atoms, [arXiv:2105.13501 \[quant-ph\]](https://arxiv.org/abs/2105.13501) (2021).
- [3] H. Levine, A. Keesling, G. Semeghini, A. Omran, T. T. Wang, S. Ebadi, H. Bernien, M. Greiner, V. Vuletić, H. Pichler, and M. D. Lukin, Parallel implementation of high-fidelity multiqubit gates with neutral atoms, *Phys. Rev. Lett.* **123**, 170503 (2019).
- [4] M. Endres, H. Bernien, A. Keesling, H. Levine, E. R. Anschuetz, A. Krajenbrink, C. Senko, V. Vuletic, M. Greiner, and M. D. Lukin, Atom-by-atom assembly of defect-free one-dimensional cold atom arrays, *Science* **354**, 1024 (2016).
- [5] D. Barredo, V. Lienhard, S. de Lésélic, T. Lahaye, and A. Browaeys, Synthetic three-dimensional atomic structures assembled atom by atom, *Nature* **561**, 79 (2018).
- [6] S. Ebadi, T. T. Wang, H. Levine, A. Keesling, G. Semeghini, A. Omran, D. Bluvstein, R. Samajdar, H. Pichler, W. W. Ho, S. Choi, S. Sachdev, M. Greiner, V. Vuletić, and M. D. Lukin, Quantum phases of matter on a 256-atom programmable quantum simulator, *Nature* **595**, 227 (2021).
- [7] P. Fendley, K. Sengupta, and S. Sachdev, Competing density-wave orders in a one-dimensional hard-boson model, *Phys. Rev. B* **69**, 075106 (2004).
- [8] G. Semeghini, H. Levine, A. Keesling, S. Ebadi, T. T. Wang, D. Bluvstein, R. Verresen, H. Pichler, M. Kalinowski, R. Samajdar, A. Omran, S. Sachdev, A. Vishwanath, M. Greiner, V. Vuletić, and M. D. Lukin, Probing topological spin liquids on a programmable quantum simulator, *Science* **374**, 1242 (2021).
- [9] C. Miles, R. Samajdar, S. Ebadi, T. T. Wang, H. Pichler, S. Sachdev, M. D. Lukin, M. Greiner, K. Q. Weinberger, and E.-A. Kim, Machine learning discovery of new phases in programmable quantum simulator snapshots, [arXiv:2112.10789 \[quant-ph\]](https://arxiv.org/abs/2112.10789) (2021).
- [10] R. Samajdar, W. W. Ho, H. Pichler, M. D. Lukin, and S. Sachdev, Complex Density Wave Orders and Quantum Phase Transitions in a Model of Square-Lattice Rydberg Atom Arrays, *Phys. Rev. Lett.* **124**, 103601 (2020).
- [11] R. Samajdar, W. W. Ho, H. Pichler, M. D. Lukin, and S. Sachdev, Quantum phases of rydberg atoms on a kagome lattice, *Proceedings of the National Academy of Sciences* **118**, e2015785118 (2021).
- [12] M. Kalinowski, R. Samajdar, R. G. Melko, M. D. Lukin, S. Sachdev, and S. Choi, Bulk and boundary quantum phase transitions in a square rydberg atom array, [arXiv:2112.10790 \[quant-ph\]](https://arxiv.org/abs/2112.10790) (2021).
- [13] R. Verresen, M. D. Lukin, and A. Vishwanath, Prediction of toric code topological order from rydberg blockade, *Phys. Rev. X* **11**, 031005 (2021).
- [14] E. Merali, I. J. S. De Vlucht, and R. G. Melko, Stochastic series expansion quantum Monte Carlo for Rydberg arrays, [arXiv:2107.00766 \[cond-mat\]](https://arxiv.org/abs/2107.00766) (2021).
- [15] W. Xu, A. V. Venkatramani, S. H. Cantú, T. Šumarac, V. Kliüsener, M. D. Lukin, and V. Vuletić, Fast Preparation and Detection of a Rydberg Qubit Using Atomic Ensembles, *Phys. Rev. Lett.* **127**, 050501 (2021).
- [16] C. Monroe, W. C. Campbell, L.-M. Duan, Z.-X. Gong, A. V. Gorshkov, P. W. Hess, R. Islam, K. Kim, N. M. Linke, G. Pagano, P. Richerme, C. Senko, and N. Y. Yao, Programmable quantum simulations of spin systems with trapped ions, *Rev. Mod. Phys.* **93**, 025001 (2021).

- [17] T. Walter, P. Kurpiers, S. Gasparinetti, P. Magnard, A. Potočnik, Y. Salathé, M. Pechal, M. Mondal, M. Oppliger, C. Eichler, and A. Wallraff, Rapid high-fidelity single-shot dispersive readout of superconducting qubits, *Phys. Rev. Applied* **7**, 054020 (2017).
- [18] G. Torlai and R. G. Melko, Learning thermodynamics with boltzmann machines, *Phys. Rev. B* **94**, 165134 (2016).
- [19] G. Carleo and M. Troyer, Solving the quantum many-body problem with artificial neural networks, *Science* **355**, 602 (2017).
- [20] G. Torlai, G. Mazzola, J. Carrasquilla, M. Troyer, R. Melko, and G. Carleo, Neural-network quantum state tomography, *Nature Physics* **14**, 447 (2018).
- [21] G. Torlai and R. G. Melko, Latent space purification via neural density operators, *Phys. Rev. Lett.* **120**, 240503 (2018).
- [22] J. Carrasquilla, G. Torlai, R. G. Melko, and L. Aolita, Reconstructing quantum states with generative models, *Nat. Mach. Intell.* **1**, 155 (2019).
- [23] M. Hibat-Allah, M. Ganahl, L. E. Hayward, R. G. Melko, and J. Carrasquilla, Recurrent neural network wave functions, *Phys. Rev. Research* **2**, 023358 (2020).
- [24] H. Ma, D. Dong, I. R. Petersen, C.-J. Huang, and G.-Y. Xiang, A comparative study on how neural networks enhance quantum state tomography, [arXiv:2111.09504 \[quant-ph\]](https://arxiv.org/abs/2111.09504) (2021).
- [25] G. Torlai, G. Mazzola, G. Carleo, and A. Mezzacapo, Precise measurement of quantum observables with neural-network estimators, *Phys. Rev. Research* **2**, 022060(R) (2020).
- [26] G. Torlai, B. Timar, E. P. L. van Nieuwenburg, H. Levine, A. Omran, A. Keesling, H. Bernien, M. Greiner, V. Vuletić, M. D. Lukin, R. G. Melko, and M. Endres, Integrating neural networks with a quantum simulator for state reconstruction, *Phys. Rev. Lett.* **123**, 230504 (2019).
- [27] G. Torlai and R. G. Melko, Machine-learning quantum states in the nisq era, *Annual Review of Condensed Matter Physics* **11**, 325 (2020).
- [28] M. Neugebauer, L. Fischer, A. Jäger, S. Czischek, S. Jochim, M. Weidemüller, and M. Gärttner, Neural-network quantum state tomography in a two-qubit experiment, *Phys. Rev. A* **102**, 042604 (2020).
- [29] K. Vogel and H. Risken, Determination of quasiprobability distributions in terms of probability distributions for the rotated quadrature phase, *Phys. Rev. A* **40**, 2847 (1989).
- [30] M. Cramer, M. B. Plenio, S. T. Flammia, R. Somma, D. Gross, S. D. Bartlett, O. Landon-Cardinal, D. Poulin, and Y.-K. Liu, Efficient quantum state tomography, *Nat. Commun.* **1**, 149 (2010).
- [31] B. P. Lanyon, C. Maier, M. Holzäpfel, T. Baumgratz, C. Hempel, P. Jurcevic, I. Dhand, A. S. Buyskikh, A. J. Daley, M. Cramer, M. B. Plenio, R. Blatt, and C. F. Roos, Efficient tomography of a quantum many-body system, *Nature Phys* **13**, 1158 (2017).
- [32] R. G. Melko, G. Carleo, J. Carrasquilla, and J. I. Cirac, Restricted Boltzmann machines in quantum physics, *Nature Physics* **15**, 887 (2019).
- [33] J. Carrasquilla and G. Torlai, How To Use Neural Networks To Investigate Quantum Many-Body Physics, *PRX Quantum* **2**, 040201 (2021).
- [34] F. Becca and S. Sorella, *Quantum Monte Carlo Approaches for Correlated Systems* (Cambridge University Press, 2017).
- [35] M. Bukov, M. Schmitt, and M. Dupont, Learning the ground state of a non-stoquastic quantum Hamiltonian in a rugged neural network landscape, *SciPost Phys.* **10**, 147 (2021).
- [36] T. Westerhout, N. Astrakhantsev, K. S. Tikhonov, M. I. Katsnelson, and A. A. Bagrov, Generalization properties of neural network approximations to frustrated magnet ground states, *Nat. Commun.* **11**, 1593 (2020).
- [37] A. Valenti, E. Greplova, N. H. Lindner, and S. D. Huber, Correlation-enhanced neural networks as interpretable variational quantum states, *Phys. Rev. Research* **4**, L012010 (2022).
- [38] M. Hibat-Allah, E. M. Inack, R. Wiersema, R. G. Melko, and J. Carrasquilla, Variational neural annealing, *Nat. Mach. Intell.* **3**, 952 (2021).
- [39] S. Morawetz, I. J. S. De Vlucht, J. Carrasquilla, and R. G. Melko, U(1)-symmetric recurrent neural networks for quantum state reconstruction, *Phys. Rev. A* **104**, 012401 (2021).
- [40] F. Ferrari, F. Becca, and J. Carrasquilla, Neural gutzwiller-projected variational wave functions, *Phys. Rev. B* **100**, 125131 (2019).
- [41] L. Viteritti, F. Ferrari, and F. Becca, Accuracy of restricted boltzmann machines for the one-dimensional j1-j2 heisenberg model, [arXiv:2202.07576 \[cond-mat.str-el\]](https://arxiv.org/abs/2202.07576) (2022).
- [42] S. Pilati, E. M. Inack, and P. Pieri, Self-learning projective quantum Monte Carlo simulations guided by restricted Boltzmann machines, *Phys. Rev. E* **100**, 043301 (2019).
- [43] C. J. Umrigar, J. Toulouse, C. Filippi, S. Sorella, and R. G. Hennig, Alleviation of the Fermion-sign problem by optimization of many-body wave functions, *Phys. Rev. Lett.* **99**, 179902(E) (2007).
- [44] E. R. Bennewitz, F. Hopfmueller, B. Kulchytskyy, J. Carrasquilla, and P. Ronagh, Neural Error Mitigation of Near-Term Quantum Simulations, [arXiv:2105.08086 \[quant-ph\]](https://arxiv.org/abs/2105.08086) (2021).
- [45] A. W. Sandvik, Stochastic series expansion method for quantum ising models with arbitrary interactions, *Phys. Rev. E* **68**, 056701 (2003).
- [46] D. Jaksch, J. I. Cirac, P. Zoller, S. L. Rolston, R. Côté, and M. D. Lukin, Fast quantum gates for neutral atoms, *Phys. Rev. Lett.* **85**, 2208 (2000).
- [47] M. D. Lukin, M. Fleischhauer, R. Cote, L. M. Duan, D. Jaksch, J. I. Cirac, and P. Zoller, Dipole blockade and quantum information processing in mesoscopic atomic ensembles, *Phys. Rev. Lett.* **87**, 037901 (2001).
- [48] S. Ahmed, C. Sánchez Muñoz, F. Nori, and A. F. Kockum, Quantum state tomography with conditional generative adversarial networks, *Phys. Rev. Lett.* **127**, 140502 (2021).
- [49] P. Cha, P. Ginsparg, F. Wu, J. Carrasquilla, P. L. McMahon, and E.-A. Kim, Attention-based quantum tomography, *Machine Learning: Science and Technology* **3**, 01LT01 (2021).
- [50] K. Cho, B. van Merriënboer, C. Gulcehre, D. Bahdanau, F. Bougares, H. Schwenk, and Y. Bengio, Learning phrase representations using RNN encoder-decoder for statistical machine translation, in *Proceedings of the 2014 Conference on Empirical Methods in Natural Lan-*

- guage Processing (EMNLP)* (Association for Computational Linguistics, Doha, Qatar, 2014) pp. 1724–1734.
- [51] D. P. Kingma and J. Ba, Adam: A method for stochastic optimization, [arXiv:1412.6980 \[cs.LG\]](https://arxiv.org/abs/1412.6980) (2014).
- [52] X. Glorot and Y. Bengio, Understanding the difficulty of training deep feedforward neural networks, in *Proceedings of the Thirteenth International Conference on Artificial Intelligence and Statistics*, Proceedings of Machine Learning Research, Vol. 9, edited by Y. W. Teh and M. Titterton (PMLR, Chia Laguna Resort, Sardinia, Italy, 2010) pp. 249–256.
- [53] G. Torlai and J. Carrasquilla, <https://github.com/gtorlai/neuralnetworks-for-quantum>, <https://github.com/gtorlai/neuralnetworks-for-quantum> (2021).